Enhancement of the creation yield of NV ensembles in a chemically vapour deposited diamond

Priyadharshini Balasubramanian, Christian Osterkamp, Ovidiu Brinza, Maxime Rollo, Isabelle Robert-Philip, Philippe Goldner, Vincent Jacques, Fedor Jelezko, Jocelyn Achard, Alexandre Tallaire

Enhancement of the creation yield of NV ensembles in a chemically vapour deposited diamond

Priyadharshini Balasubramanian[a], Christian Osterkamp[a], Ovidiu Brinza[b], Maxime Rollo[c], Isabelle Robert-Philip[c], Philippe Goldner[d], Vincent Jacques[c], Fedor Jelezko[a], Jocelyn Achard[b], Alexandre Tallaire[d*]

[a] *Institute for Quantum Optics and Center for Integrated Quantum Science and Technology (IQST), Ulm University, 89081 Ulm, Germany*

[b] *Laboratoire des Sciences des Procédés et des Matériaux, LSPM, CNRS, Université Sorbonne Paris-Nord, Villetaneuse 93430, France*

[c] *Laboratoire Charles Coulomb, Université de Montpellier, CNRS, Montpellier 34095, France*

[d] *Institut de Recherche de Chimie Paris, IRCP, Chimie ParisTech, PSL University, CNRS, Paris 75005, France*

ABSTRACT

In this work we investigate the properties of nitrogen-vacancy (NV) centres created during single crystal diamond growth by Chemical Vapour Deposition (CVD) on [113]-oriented substrates and with N_2O as a dopant gas. The use of spin echo and double electron-electron resonance (DEER) allows us to assess NV ratio with respect to substitutional nitrogen impurities (N_s), a critical parameter to optimize for quantum technologies. We demonstrate that, at moderate growth temperatures (800 °C), dense NV ensembles of several hundreds of ppb (800 ppb for 50 ppm of added N_2O) with exceptionally high NV/N_s creation yields of up to 25 % can be achieved. This value is higher by at least an order of magnitude to that typically obtained on standard [100]-grown diamonds and comparable to electron irradiated diamonds under optimized conditions. The material obtained here thus advantageously combines a high NV density, high yield, long coherence times of several tens of µs together with preferential orientation of around 70 %. These are highly desirable requirements for diamond-based quantum sensors that may spur new developments with this crystalline orientation leading to improved performance and sensitivity.

Keywords:

* Corresponding author : Phone: +33 1 85 78 42 31; Email: alexandre.tallaire@chimieparistech.psl.eu

Colour centres in diamond, quantum technologies, CVD growth, NV yield, single crystal diamond

Highlights:

- Dense NV ensembles up to 800 ppb obtained on [113]-oriented diamond with N_2O as a dopant
- Low temperature growth promotes nitrogen incorporation in the NV form
- NV/N_s creation yield measured by double electron-electron resonance.
- Highest yield ever obtained of 25 %.

1. Introduction

Diamond is one the most promising solid-state material system for the emerging field of quantum technologies, in particular quantum sensing. One of its colour centres, the negatively charged nitrogen-vacancy (NV) defect, features optically addressable electronic spin states with exceptionally long coherence times up to room temperature [1]. These electron spin states are already used as a quantum sensor, allowing the measurement and imaging of temperature [2], pressure [3], strain [4,5], magnetic [6,7] and electric fields [8] with nanoscale precision and exceptional sensitivity. Over the years, NV-based diamond sensors have become useful tools to address a wide range of applications and to investigate systems that would otherwise be inaccessible to conventional sensors. For example it has opened new avenues in studying exotic spin textures in condensed matter physics [9], analysing current flows in electronic devices [10] or following the mechanisms occurring inside living cells in biology [11].

NV-based quantum technology progresses have been mostly driven by the availability of engineered diamond material produced by plasma assisted Chemical Vapour Deposition (CVD) [12]. As a growth technique, CVD offers several crucial advantages. By precisely controlling the gas phase environment and the growth parameters, the chemical composition of the films can be controlled down to the ppb range [13]. The nuclear spin bath originating from ^{13}C can be reduced using isotopically ^{12}C-enriched methane as a growth precursor [14]. NV centres with excellent spin properties can also be intentionally incorporated during growth in a narrow layer close to the surface by reducing the diamond growth rates [15,16] or by harnessing the temperature dependence of NV incorporation [17]. This brings the possibility to address NVs in a spatially constrained region and further facilitates the development of quantum sensors. An additional benefit, unique to CVD, is the ability to promote a specific crystalline orientation for NV centres [18–20]. While growth on conventional [100]-oriented substrates leads to a random distribution between the four <111> directions, growth on [113]-oriented diamonds provides up to 80 % preferential orientation along a single direction [18], particularly when growth is carried out at moderate temperatures [21]. In this case, a specific NV population can be addressed resulting in improved magnetic sensitivity.

For many sensing applications, it is also important to increase NV density in order to interrogate a higher number of spins [22] which leads to improved sensitivities. Obtaining dense NV ensembles by direct in-situ doping is however hampered by the low N incorporation efficiency in diamond

(typically 10^{-3} to 10^{-5}) [13] and a degraded surface morphology under high N_2 concentrations (> 100 ppm in the gas phase) [23]. By using an alternative dopant gas such as N_2O, it is possible to include higher amounts of nitrogen before reaching degraded morphologies while better photostability of the colour centres was observed [24]. However, achievable NV concentrations are still relatively limited to a few hundreds of ppb [25]. Typically, the NV to substitutional nitrogen (N_s) yield (NV/N_s) is as low as 1/300 when growth is performed on conventional [100]-oriented diamond substrates [26,27]. This means that most of the nitrogen is present as single isolated atoms. Such N_s impurities, known as P1 centres in Electron Paramagnetic Resonance (EPR) spectroscopy, significantly contribute to the spin bath noise [28]. Increasing NV density leads to higher N_s concentrations which comes at the expense of a reduced spin coherence time particularly when nitrogen exceeds a few ppm in the crystal [29].

A few alternatives have been proposed to improve NV yield beyond that typically reached after growth. Recently, a creation yield close to 1/100 has for example been reported for specific growth conditions on a [111] orientation [30]. High energy electron or neutron irradiation may also be used to introduce additional vacancies in the diamonds and thus convert part of the nitrogen in the sample into useful NV centres [25,31]. After annealing, yields up to 20 % have been reached. These post-treatments however usually require heavy equipment and lead to random orientation of the defects. The possibility to obtain high NV yields and preferential orientation by direct CVD growth would thus represent an important advantage.

In a previous work [21], a relatively high NV density with improved preferential orientation was obtained by growing at lower growth temperatures (around 800 °C) on [113]-oriented CVD diamond. This high density may arise from a higher NV creation yield or, more generally a higher N incorporation. To identify the underlying process at play, we here rely on spin echo and double electron-electron resonance (DEER) [32] to elucidate the dependence of NV/N_s ratio on growth conditions. We first confirm that low temperature promotes the incorporation of nitrogen in the NV form. We then extend this investigation to the synthesis of dense NV ensembles (300-800 ppb) on a [113]-diamond using intentional addition of N_2O. We reach an exceptionally high creation yield of up to 25 %, which represents more than an order of magnitude improvement compared to conventional [100]-growth. This result compares to that reached with optimized irradiation [25] but without imparting coherent properties and avoiding costly and time consuming engineering steps.

2. Material and methods

We used commercial High-Pressure High-Temperature (HPHT) type *Ib* substrates that were laser cut and polished so that their main top face is oriented along the [113] direction, as described in reference [18]. Diamond growth was performed at LSPM in a home-made plasma-assisted CVD system under typical pressure and microwave power conditions of 180-250 mbar and 2800-3500 W [33]. The first homoepitaxial film (sample 1) was grown in a continuous run with only background nitrogen impurities in the chamber (i.e. < 1 ppm) but the growth temperature was varied periodically between 800 and 1000 °C by adjusting the power and pressure in the chamber [21]. The second homoepitaxial film (sample 2) was grown at a constant and moderate temperature of 800-830 °C but with varying nitrogen addition. It was composed of 4 layers (Fig. 2a). Layer A was non-intentionally doped while for layers B, C and D, 10, 20 and 50 ppm of N_2O were added, respectively. Each layer was about 30-40 µm thick. Both samples were eventually laser cut and polished on their lateral sides to facilitate cross-section analysis.

Raman and photoluminescence (PL) analysis were carried out using a *Horiba HR800* experimental set-up that uses a 473 nm excitation laser line. An automated scanning stage was used to record maps of the PL across the sample's cross-section. All the optical and spin characterization experiments were performed in a home-built confocal microscope. The NV centres were excited using a 532nm laser through a high numerical aperture objective (NA 1.35). The same objective collected the resulting PL signal from NV centres which were then detected using an avalanche photodiode. Neutral density filters were placed in the detection path to attenuate the fluorescence intensity from the ensembles in order to avoid saturation of the APD. A 20 µm diameter copper wire was placed above the sample to apply the microwave field necessary for performing optically detected electron spin resonance (ESR) spectroscopy. In order to reject common-mode noise like laser fluctuations, all the pulsed ESR experiments were carried with two consecutive identical experiments that projected the final NV spin state onto the $m_s = 0$ spin sublevel (with fluorescence F_0) and onto the $m_s = 1$ sublevel (with fluorescence F_1) with proper choice of the readout π/2-pulse. The plotted results were obtained as $(F_0-F_1) / (F_0+F_1)$.

For the P1 density measurement, we used the time-swept DEER sequence, where the P1 bath pulse is applied at each of the P1 transition frequency (or P1 groups) and the corresponding decay is recorded. The total P1 density is then calculated as $n_{P1} = \sum_{\mathrm{group=i}}^{\mathrm{v}} n_{\mathrm{group}}$. When this is tedious due to long measurement times, the total P1 density is calculated as $n_{P1} = n_{\mathrm{iii}} + 2\, n_{\mathrm{iv}} + +2\, n_{\mathrm{v}}$. Alternatively, one could just measure the decay due to P1 - group v, and the total P1 density is $n_{P1} = 12\, n_{\mathrm{v}}$.

For the NV concentration estimation, we compared the time-averaged fluorescence intensity rate in the different growth layers with the fluorescence rate measured from single NV centres under the same experimental conditions (power and polarization of the excitation laser and adjustment of spectral detection window). In order to confirm that the fluorescence spot indeed host only a single NV centre, we used Hanbury Brown and Twiss interferometry setup to measure the second-order correlation function.

3. Results and discussion

The first multilayer sample studied here was grown on a [113]-oriented diamond without intentional nitrogen addition under a variable temperature between 800 and 1000 °C. An image of the sample and the PL map acquired in cross-section are presented in Fig. S1 of the supplementary information file. Two of these layers grown under high or low temperature (labelled HT and LT layers) are considered in the magnified PL image of Fig. 1a. We confirmed that the high temperature layers incorporated less NV centres than the low temperature ones. Based on the PL intensity measured for single NV centres isolated in the high-temperature layer, we were able to estimate the NV density in the low temperature layers to about 4.5 ppb. An example of such a single NV centre, as demonstrated by the autocorrelation measurement, is given in Fig. S2 of the supplementary information file. Spin echo measurements (Fig. 1b) were then performed on single NVs in the HT layer (orange) and on the NV ensembles in the LT layer (blue). A T_2 coherence time of approximately 250 µs was found for both layers. This fairly long value is expected in this low NV doping range in which decoherence is mostly driven by the ^{13}C nuclear spin bath [29].

In order to evaluate the source of magnetic noise, echo-based DEER measurements were eventually carried out on both layers (Fig. 1c and d). To this end, we used the NV centres hosted in these layers as probe spins, to quantify their local magnetic environment. The echo-based DEER pulse sequence combines a simple spin echo on the NV centre with a selective inversion of the bath spins. With this sequence, the NV centre recouples to the static magnetic environment that is inverted by the bath spin π-pulse, leading to an observable decrease in the NV echo amplitude. Figure 1c, shows the frequency swept DEER sequence used to obtain the P1 bath transition frequencies along with the P1 spectrum measured on the LT layer at an external field of B_0 = 666 G aligned along the <111> direction. The measured spectrum resembles the characteristic P1 spectrum for ^{14}N isotope [34].

In order to benchmark the grown material, we use the technique presented in [30]. The density of P1 bath spins is measured by using pulse sequence shown in Fig.1d. Here the π-pulse on the bath spins (addressing one of the P1 transition) is swept in time with respect to the NV echo readout π/2-

pulse. By sweeping the bath inversion pulse in time, we reintroduce the NV-P1 interaction, leading to the decay of the NV coherence depending on the density of the inverted spins (n_{P1}) and the recoupling time T. The P1 bath density for the different groups and for both the LT and HT layers are given in Fig. S3 of the supplementary information file. In Fig. 1d, we plot the NV echo amplitude as a function of the recoupling time T for HT and LT layers (orange and blue) when the bath π-pulse is applied on the centre transition of the P1 spectrum (indicated as (iii) in Fig. 1c). The DEER experiment is repeated for each of the P1 transitions and the measured data is fitted with the function of the form $\exp[-A\,\gamma_{NV}\gamma_{P1}n_{P1}T]$, where $A\,\gamma_{NV}\gamma_{P1}\sim 292$ kHz/ppm [35]. For both layers, similar values of 120-200 ppb were extracted. This corresponds to an NV creation yield (i.e. NV/N_s) as high as 3 % for the low-temperature growth. This clearly indicates that the combination of [113] growth and low temperature promotes NV incorporation without significantly affecting the total substitutional nitrogen incorporation. This is a particularly favourable situation to obtain higher NV densities with maximized coherence and improved properties for quantum applications.

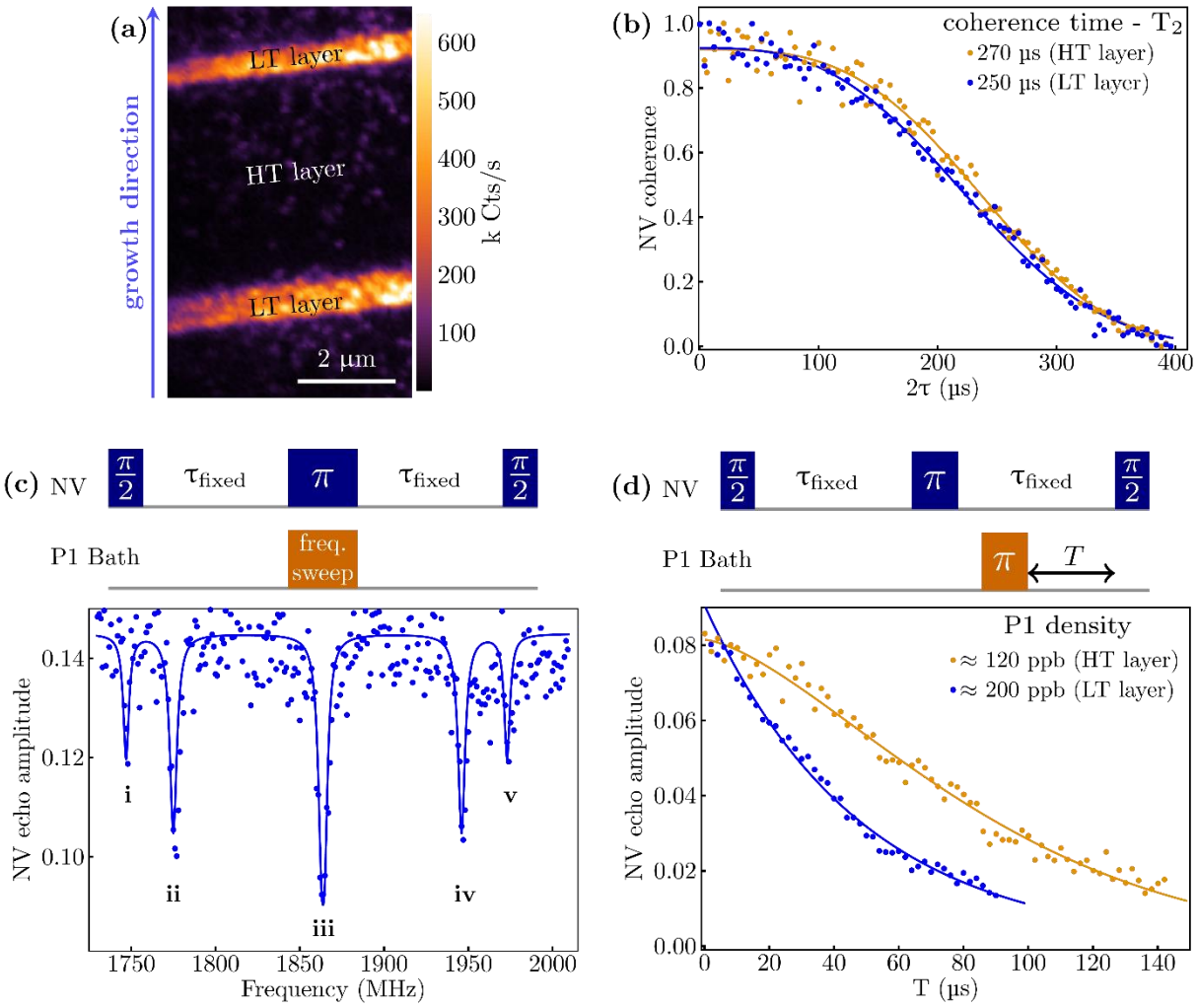

Figure 1 (a) Confocal PL microscopy image of a [113] CVD diamond multilayer (sample 1) seen in cross-section. The luminescent LT layer was grown at 800 °C while the dark region (HT layer) corresponds to growth at 1000°C. Only background N_2 was present in the gas phase. The arrow indicates the growth direction. (b) Spin echo of NV centres in HT and LT layers, showing a T_2 coherence of about 250 µs. (c) Frequency swept DEER spectrum of LT layer along with the pulse sequence. The measurement is performed at an external magnetic field of 666 G aligned along the <111> crystal direction. The inter-pulse spacing in the echo sequence is fixed at 25 µs. (d) Time swept DEER sequence for measuring the P1 density. The bath π-pulse is applied at the centre transition frequency (marked by (iii) in c) of the P1 spectrum. The inter pulse spacing (τ_{fixed}) is kept as 150 µs and 100 µs for HT and LT layers, respectively. For HT and LT layers, we measure P1 bath concentrations of 120 and 200 ppb respectively.

In order to extend this result to the creation of dense NV ensembles, we prepared a second sample (sample 2), also on a [113]-oriented substrate and under low temperature conditions, but with intentional doping during growth using various amounts of N_2O from 0 to 50 ppm. This multilayer sample was observed in cross-section under transmitted white light (Fig. 2a). The different stacked

layers can be clearly distinguished as they exhibit pink to dark colour from the lowest to highest doping levels. This colour is noteworthy as growth on [100]-oriented diamonds with high nitrogen doping is more likely to lead to a brown colouration originating from a large amount of absorbing defects such as aggregated vacancies [36]. This is already a first hint that NV centres are a dominating impurity in our case which would support our previous statement.

PL spectra acquired for the different layers along the cross-section are also presented in Fig. 2b. For layers B, C and D, three strong emissions corresponding to NV^0, NV^- and SiV^- at 575, 637 and 737 nm respectively are observed. Their intensity variation is reported in Fig. 2c. As expected, NV emission of both charge states increase with N_2O doping but show saturation for the highest doping level (50 ppm). On the other hand, SiV^- emission starts to increase as soon as nitrogen is incorporated but remains relatively stable afterwards. This is consistent with the fact that nitrogen is an electron donor that promotes the negative charge state of SiV. Silicon impurities originate from contamination inside the growth chamber (quartz windows essentially) and are thus a relatively constant background impurity during the growth run.

The diamond Raman peak's Full Width at Half Maximum (FWHM) and peak position around 1332 cm^{-1} also provide information on the crystalline quality and the presence of strain in the films (Fig. 2d and 2e). We can see that the diamond Raman line is narrower in the CVD layers (A-C) as compared to the HPHT substrate (S) that contains a higher amount of impurities. Layer D differs from the others with a much higher FWHM (around 3 cm^{-1}). Similar observation can be made with respect to the peak position that is nearly constant for all layers except for layer D that shows a drastic drop. This is consistent with the fact that, at this doping level (50 ppm in the gas phase), the crystalline quality substantially worsens, and strain starts to be generated. This would set the ideal maximum doping range to between 20 and 50 ppm of N_2O in the gas phase on this orientation, in order to get high NV density with limited strain.

In order to see if the preferential orientation expected on this orientation is retained for higher density ensembles, we also measured ODMR spectrum for the middle layer (layer C) using a randomly oriented magnetic field of 40 G. We observed only 3 pairs of resonances corresponding to 3 NV families with the most in-plane direction being undetectable. To the contrary the most out-of-plane direction corresponding to the 2 most extreme peaks in the ODMR spectrum is promoted. We thus confirm the partial preferential orientation already shown for lower NV densities [18] although we could not precisely quantify it in this case. The measured contrast for the different resonances is however consistent with our previous results on isolated single centres, suggesting

values around 70 %. This is different from [111]-oriented growth in which a loss of preferential orientation was observed when growing dense ensembles [37].

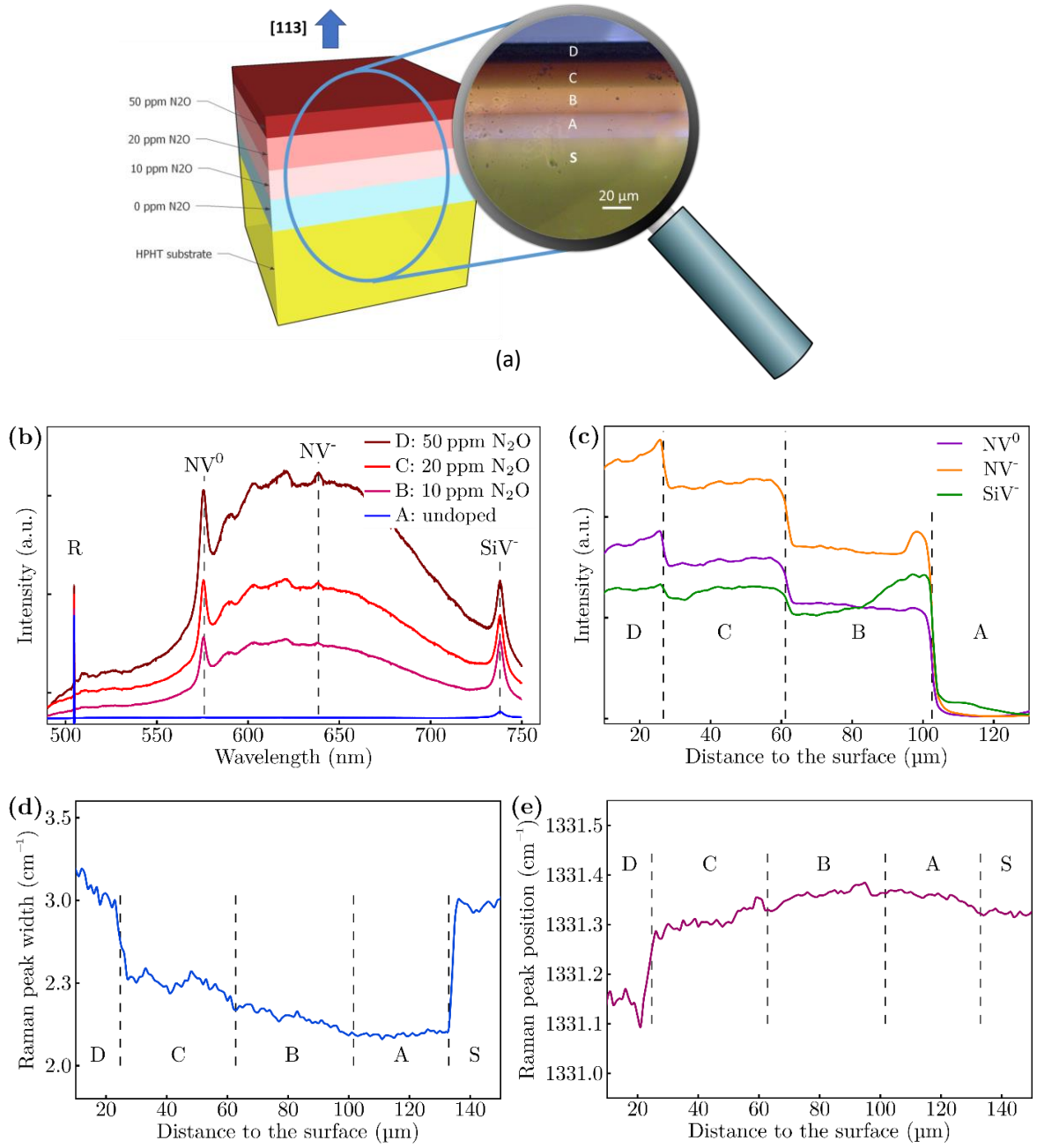

Figure 2. (a) Schematic of the multilayer structure (sample 2) grown with an increasing amount of N_2O. The inset shows an optical microscopy image of the sample's cross section under transmitted white light. (b) Raman/PL spectra acquired along the cross-section with a 473 nm laser line. The position of NV^0, NV^- and SiV^- peaks are identified by the dotted lines and numbered 1-3 while the diamond Raman peak is labelled R. Spectra are normalized to the Raman peak and vertically shifted for clarity. (c) PL profile along the cross-section reporting the intensity of PL emissions from the top layer (D) to the interface (A). (d) Diamond Raman peak's width and (e) Diamond Raman peak position measured along the cross-section of the multilayer sample.

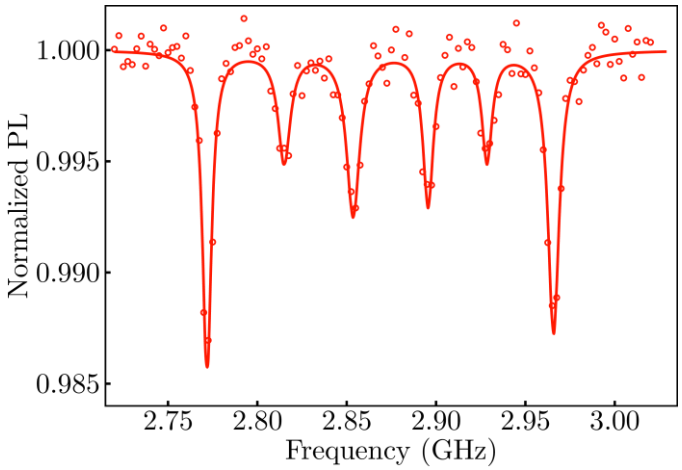

Figure 3. Optically detected ESR spectrum acquired for the layer D grown with 40 ppm of N_2O in the multilayer structure (sample 2). The spectrum was recorded under a randomly oriented magnetic field of about 40 G. Different pairs of resonances corresponding to 3 NV families are observed with one of them being dominant, which is a signature of a preferential orientation of NV defects.

Eventually, we assessed the creation yield of NV centres in this highly doped multilayer sample. Figure 4a shows the confocal microscopy PL image of the multilayer sample attenuated and filtered in the wavelength range 560-1000 nm, along the sample cross-section. By comparison with the fluorescence count from a single NV centre, we evaluated the NV density in each layer from the recorded PL intensity. The filtering procedure used is illustrated in Fig. S4 of the supplementary information file. The calculated values, presented in Table 1, confirm an increase of NV density with N_2O addition and a saturation for doping above 20 ppm. Several hundreds of ppb of NV centres were successfully incorporated in the films which represents a significant amount for an as-grown (i.e. non-irradiated) diamond sample.

In order to evaluate NV coherence properties, we used the Hahn echo sequence to measure the spin echo coherence time (T_2). A magnetic field of 600 G was aligned along the <111> crystal direction. The coherence time was evaluated for each layer, where the difference between a $\pi/2$ and a $3\pi/2$ readout was plotted to exclude artefacts. Representing examples of such measurements are provided in Fig. 4b. The results are reported in Table 1. T_2 reduces from about 35 to 6 µs from layer B to layer D. If we assume that in these highly doped samples, decoherence is mostly driven by the electronic spin bath from nitrogen atoms, we expect that the total nitrogen concentration is between 1 and 10 ppm, based on the data reported in reference [29].

In order to more precisely quantify the P1 spin bath density, we performed spin-echo based double electron-electron resonance (DEER) [38] for the 3 layers. The DEER pulse sequence and the experimental details are the same as those mentioned above. The results are reported in Fig. 4c-d and summarized in Table 1 for all layers. For layer B, we measured a P1 density of about 1 ppm while NV concentration was estimated to 358 ppb. Based on this, an NV creation yield $n_{NV}/(n_{NV} + n_{P1})$ above 25 % can be calculated which is to our knowledge the highest value reported so far, for a non-irradiated sample. For the other 2 layers with a higher NV doping, the creation yield is slightly reduced but remains high, above 20 %. This yield is improved by an order of magnitude with respect to conventional [100]-oriented growth [26]. In addition, we evaluated the total nitrogen doping efficiency which represents the fraction of N incorporated in the film with respect to that present in the gas phase. We found efficiencies of up to 0.07 that slightly decrease with the amount of N_2O introduced. These values are also higher than those typically reported on [100]-oriented films grown under similar conditions and high plasma power densities (typically 10^{-3} to 10^{-5}) [13]. We infer that this high NV yield and N incorporation efficiency relate to the combined use of [113] orientation and moderate growth temperature.

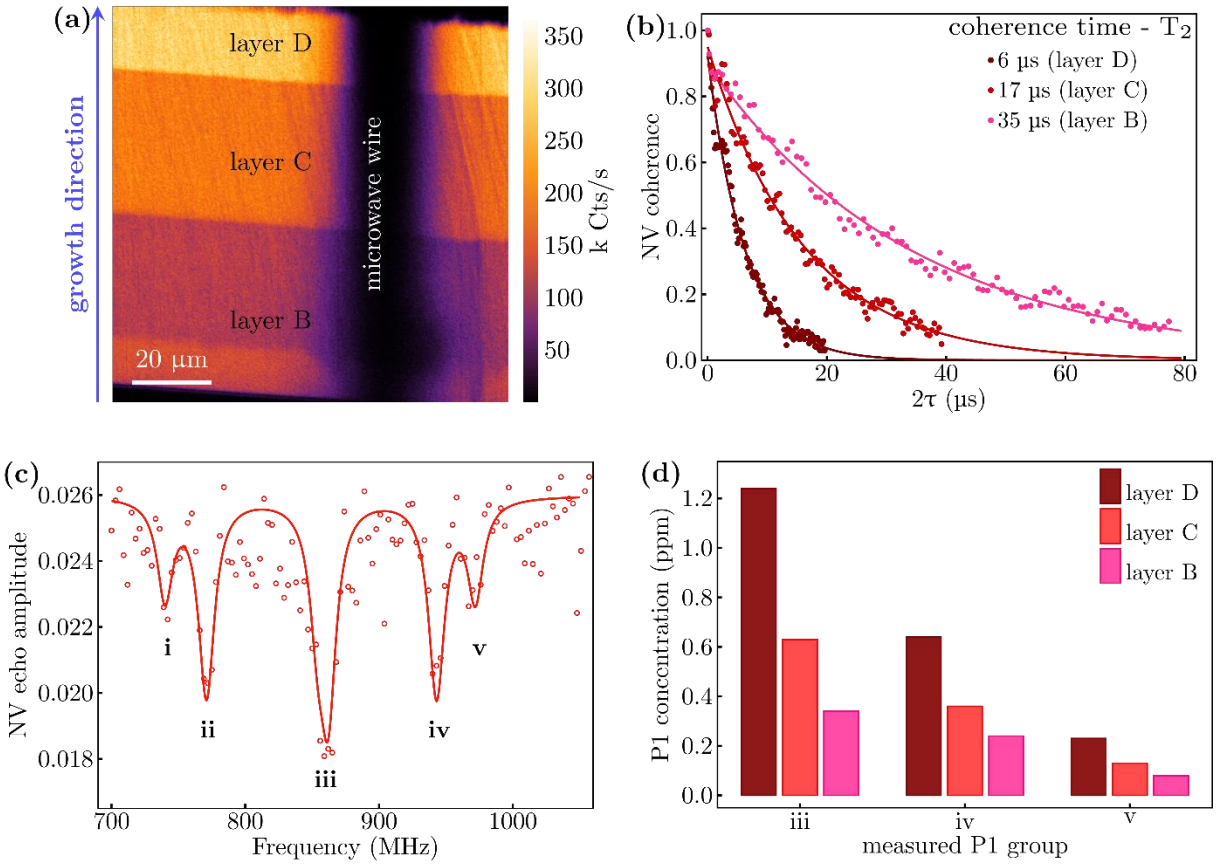

Figure 4. *(a) Confocal microscopy PL image along the cross-section of sample 2 from which the 3 layers can be clearly distinguished. The shaded line in the middle corresponds to the wire used to apply microwaves and drive spin transitions. (b) Spin echo measurement of the 3 layers. (c) DEER spectrum obtained for layer C at an external magnetic field of 310 G aligned along the <111> crystal axis. The spectrum is obtained with NV echo inter-pulse spacing fixed at 3µs. (d) Comparison of P1 spin bath concentration measured on different P1 groups for layer D, C and B. The corresponding DEER measurement data is shown in Fig. S5 of the supplementary information file.*

Table 1. Distribution of nitrogen and NV properties in the multilayer diamond (sample 2). The total nitrogen incorporation efficiency and NV creation yield are calculated from the experimental results.

	Layer B	**Layer C**	**Layer D**
N_2O addition (ppm)	10	20	50
PL count rate (Mcps/s)	70	101	134
NV density (ppb)	358	530	835
T_2 echo (µs)	35±3	16.8±0.7	6.1±0.3
P1 density (ppm)	1.03±0.02	1.6±0.05	2.98±0.12
Total N incorporation efficiency ($N_{crystal}/N_{gas}$)	0.069	0.053	0.033
NV yield (%)	25.8	24.9	21.9

4. Conclusions

In summary, we investigated the properties of NV centres created on [113]-oriented CVD diamonds using N_2O as a dopant in the gas phase. In particular, we focused on maximizing the NV/N_s ratio in dense ensembles since the presence of a high amount of unwanted paramagnetic N_s impurities strongly affects the achievable coherence times in this material. We found that on this crystalline orientation and under moderate growth temperatures, high NV densities of up to 800 ppb can be obtained without seriously impacting the crystalline quality. Furthermore, the diamond films produced exhibited an extremely high $n_{NV}/(n_{NV}+n_{P1})$ creation yield of up to 25 % with preserved coherence times of a few tens of µs. Such high yields in bulk as-grown crystals are unique to this [113] material orientation and can hardly be achieved even using post-growth irradiation with high energy electron or proton beams for example. In addition, while post-treatment irradiation leads to the creation of additional lattice damage and random orientation of NV defects among the 4 different NV families, our growth approach advantageously offers around 70 % preferential orientation in a single orientation. The results presented here will likely open perspectives in exploiting high NV-doped [113] CVD diamonds for the development of quantum sensors with extended performance in terms of sensitivity and practicability.

Credit authorship statement:

P. Balasubramanian: Investigation, Writing - Review & Editing, **C. Osterkamp:** Investigation, Writing - Review & Editing, **O. Brinza:** Investigation, **M. Rollo:** Investigation, **I. Robert-Philip:** Writing - Review & Editing, **P. Goldner:** Writing - Review & Editing, **V. Jacques:** Conceptualization, **F. Jelezko:** Supervision, **J. Achard:** Supervision, **A. Tallaire:** Writing - Original Draft, Conceptualization

Acknowledgements:

This work has received funding from the European Union's research and innovation program through the ASTERIQS project under grant agreement n° 820394, the Quantera initiative (MICROSENS project ANR-18-QUAN-0008-02) and the Diamond-NMR project n° ANR-19-CE29-0017-04. The work was also supported by the Ile-de-France region in the framework of DIM SIRTEQ. ANR (Agence Nationale de la Recherche) and CGI (Commissariat à l'Investissement d'Avenir) are also gratefully acknowledged for their financial support through Labex SEAM (Science and Engineering for Advanced Materials and devices): ANR-10-LABX-096 and ANR-18-IDEX-0001.

References

[1] M.W. Doherty, N.B. Manson, P. Delaney, F. Jelezko, J. Wrachtrup, L.C.L. Hollenberg, The nitrogen-vacancy colour centre in diamond, Physics Reports. 528 (2013) 1–45. http://dx.doi.org/10.1016/j.physrep.2013.02.001.

[2] G. Kucsko, P.C. Maurer, N.Y. Yao, M. Kubo, H.J. Noh, P.K. Lo, H. Park, M.D. Lukin, Nanometre-scale thermometry in a living cell, Nature. 500 (2013) 54–58. https://doi.org/10.1038/nature12373.

[3] M. Lesik, T. Plisson, L. Toraille, J. Renaud, F. Occelli, M. Schmidt, O. Salord, A. Delobbe, T. Debuisschert, L. Rondin, P. Loubeyre, J.-F. Roch, Magnetic measurements on micrometer-sized samples under high pressure using designed NV centers, Science. 366 (2019) 1359–1362. https://doi.org/10.1126/science.aaw4329.

[4] P. Kehayias, M.J. Turner, R. Trubko, J.M. Schloss, C.A. Hart, M. Wesson, D.R. Glenn, R.L. Walsworth, Imaging crystal stress in diamond using ensembles of nitrogen-vacancy centers, Phys. Rev. B. 100 (2019) 174103. https://doi.org/10.1103/PhysRevB.100.174103.

[5] D.A. Broadway, B.C. Johnson, M.S.J. Barson, S.E. Lillie, N. Dontschuk, D.J. McCloskey, A. Tsai, T. Teraji, D.A. Simpson, A. Stacey, J.C. McCallum, J.E. Bradby, M.W. Doherty, L.C.L. Hollenberg, J.-P. Tetienne, Microscopic Imaging of the Stress Tensor in Diamond Using in Situ Quantum Sensors, Nano Lett. 19 (2019) 4543–4550. https://doi.org/10.1021/acs.nanolett.9b01402.

[6] L. Rondin, J.P. Tetienne, T. Hingant, J.-F. Roch, P. Maletinsky, V. Jacques, Magnetometry with nitrogen-vacancy defects in diamond, Reports on Progress in Physics. 77 (2014) 056503.

[7] J.F. Barry, J.M. Schloss, E. Bauch, M.J. Turner, C.A. Hart, L.M. Pham, R.L. Walsworth, Sensitivity optimization for NV-diamond magnetometry, Rev. Mod. Phys. 92 (2020) 015004. https://doi.org/10.1103/RevModPhys.92.015004.

[8] F. Dolde, H. Fedder, M.W. Doherty, T. Nöbauer, F. Rempp, G. Balasubramanian, T. Wolf, F. Reinhard, L.C.L. Hollenberg, F. Jelezko, J. Wrachtrup, Electric-field sensing using single diamond spins, Nature Phys. 7 (2011) 459–463. https://doi.org/10.1038/nphys1969.

[9] I. Gross, W. Akhtar, V. Garcia, L.J. Martínez, S. Chouaieb, K. Garcia, C. Carrétéro, A. Barthélémy, P. Appel, P. Maletinsky, J.-V. Kim, J.Y. Chauleau, N. Jaouen, M. Viret, M. Bibes, S. Fusil, V. Jacques, Real-space imaging of non-collinear antiferromagnetic order with a single-spin magnetometer, Nature. 549 (2017) 252–256. https://doi.org/10.1038/nature23656.

[10] J.-P. Tetienne, N. Dontschuk, D.A. Broadway, A. Stacey, D.A. Simpson, L.C.L. Hollenberg, Quantum imaging of current flow in graphene, Science Advances. 3 (2017) e1602429. https://doi.org/10.1126/sciadv.1602429.

[11] D.R. Glenn, D.B. Bucher, J. Lee, M.D. Lukin, H. Park, R.L. Walsworth, High-resolution magnetic resonance spectroscopy using a solid-state spin sensor, Nature. 555 (2018) 351. https://doi.org/10.1038/nature25781 https://www.nature.com/articles/nature25781#supplementary-information.

[12] J. Achard, V. Jacques, A. Tallaire, CVD diamond single crystals with NV centres: a review of material synthesis and technology for quantum sensing applications, J. Phys. D: Appl. Phys. (2020). https://doi.org/10.1088/1361-6463/ab81d1.

[13] A. Tallaire, A.T. Collins, D. Charles, J. Achard, R. Sussmann, A. Gicquel, M.E. Newton, A.M. Edmonds, R.J. Cruddace, Characterisation of high-quality thick single-crystal diamond grown by CVD with a low nitrogen addition, Diam. & Relat. Mat. 15 (2006) 1700–1707. https://doi.org/10.1016/j.diamond.2006.02.005.

[14] G. Balasubramanian, P. Neumann, D. Twitchen, M. Markham, R. Kolesov, N. Mizuochi, J. Isoya, J. Achard, J. Beck, J. Tissler, V. Jacques, P.R. Hemmer, F. Jelezko, J. Wrachtrup, Ultralong spin coherence time in isotopically engineered diamond, Nat Mater. 8 (2009) 383–387.

[15] K. Ohno, F. Joseph Heremans, L.C. Bassett, B.A. Myers, D.M. Toyli, A.C. Bleszynski Jayich, C.J. Palmstrom, D.D. Awschalom, Engineering shallow spins in diamond with nitrogen delta-doping, Applied Physics Letters. 101 (2012) 082413.

[16] Christian Osterkamp, Johannes Lang, Jochen Scharpf, Christoph Müller, Liam Paul McGuinness, Thomas Diemant, R. Jürgen Behm, Boris Naydenov, Fedor Jelezko, Stabilizing shallow color centers in diamond created by nitrogen delta-doping using SF6 plasma treatment, Applied Physics Letters. 106 (2015) 113109. https://doi.org/10.1063/1.4915305.

[17] A. Tallaire, M. Lesik, V. Jacques, S. Pezzagna, V. Mille, O. Brinza, J. Meijer, B. Abel, J.F. Roch, A. Gicquel, J. Achard, Temperature dependent creation of nitrogen-vacancy centers in single crystal CVD diamond layers, Diam. & Relat. Mat. 51 (2015) 55–60.

[18] M. Lesik, T. Plays, A. Tallaire, J. Achard, O. Brinza, L. William, M. Chipaux, L. Toraille, T. Debuisschert, A. Gicquel, J.F. Roch, V. Jacques, Preferential orientation of NV defects in CVD diamond films grown on (113)-oriented substrates, Diam. & Relat. Mat. 56 (2015) 47–53.

[19] J. Michl, T. Teraji, S. Zaiser, I. Jakobi, G. Waldherr, F. Dolde, P. Neumann, M.W. Doherty, N.B. Manson, J. Isoya, J. Wrachtrup, Perfect alignment and preferential orientation of nitrogen-vacancy centers during chemical vapor deposition diamond growth on (111) surfaces, Appl. Phys. Lett. 104 (2014) 102407. https://doi.org/doi:http://dx.doi.org/10.1063/1.4868128.

[20] M. Lesik, J.P. Tetienne, A. Tallaire, J. Achard, V. Mille, A. Gicquel, J.F. Roch, V. Jacques, Perfect preferential orientation of nitrogen-vacancy defects in a synthetic diamond sample, Appl. Phys. Lett. 104 (2014) 113107. https://doi.org/doi:http://dx.doi.org/10.1063/1.4869103.

[21] S. Chouaieb, L.J. Martínez, W. Akhtar, I. Robert-Philip, A. Dréau, O. Brinza, J. Achard, A. Tallaire, V. Jacques, Optimizing synthetic diamond samples for quantum sensing technologies by tuning the growth temperature, Diam. & Relat. Mat. 96 (2019) 85–89. https://doi.org/10.1016/j.diamond.2019.04.022.

[22] A.M. Edmonds, C.A. Hart, M.J. Turner, P.-O. Colard, J.M. Schloss, K. Olsson, R. Trubko, M.L. Markham, A. Rathmill, B. Horne-Smith, W. Lew, A. Manickam, S. Bruce, P.G. Kaup, J.C. Russo, M.J. DiMario, J.T. South, J.T. Hansen, D.J. Twitchen, R. Walsworth, Characterisation of CVD diamond with high concentrations of nitrogen for magnetic-field sensing applications, Mater. Quantum. Technol. (2021). https://doi.org/10.1088/2633-4356/abd88a.

[23] J. Achard, F. Silva, O. Brinza, A. Tallaire, A. Gicquel, Coupled effect of nitrogen addition and surface temperature on the morphology and the kinetics of thick CVD diamond single crystals, Diam. & Relat. Mat. 16 (2007) 685–689.

[24] A. Tallaire, L. Mayer, O. Brinza, M.A. Pinault-Thaury, T. Debuisschert, J. Achard, Highly photostable NV centre ensembles in CVD diamond produced by using N2O as the doping gas, Applied Physics Letters. 111 (2017) 143101. https://doi.org/10.1063/1.5004106.

[25] A. Tallaire, O. Brinza, P. Huillery, T. Delord, C. Pellet-Mary, R. Staacke, B. Abel, S. Pezzagna, J. Meijer, N. Touati, L. Binet, A. Ferrier, P. Goldner, G. Hetet, J. Achard, High NV density in a pink CVD diamond grown with N2O addition, Carbon. 170 (2020) 421–429. https://doi.org/10.1016/j.carbon.2020.08.048.

[26] A.M. Edmonds, U.F.S. D'Haenens-Johansson, R.J. Cruddace, M.E. Newton, K.M.C. Fu, C. Santori, R.G. Beausoleil, D.J. Twitchen, M.L. Markham, Production of oriented nitrogen-vacancy color centers in synthetic diamond, Physical Review B. 86 (2012) 035201.

[27] T. Luo, L. Lindner, J. Langer, V. Cimalla, F. Hahl, C. Schreyvogel, S. Onoda, S. Ishii, T. Ohshima, D. Wang, D.A. Simpson, B.C. Johnson, M. Capelli, R. Blinder, J. Jeske, Creation of nitrogen-vacancy centers in chemical vapor deposition diamond for sensing applications, ArXiv:2111.07981 [Cond-Mat, Physics:Physics, Physics:Quant-Ph]. (2021). http://arxiv.org/abs/2111.07981 (accessed November 16, 2021).

[28] N. Bar-Gill, L.M. Pham, C. Belthangady, D. Le Sage, P. Cappellaro, J.R. Maze, M.D. Lukin, A. Yacoby, R. Walsworth, Suppression of spin-bath dynamics for improved coherence of multi-spin-qubit systems, Nat Commun. 3 (2012) 858.

[29] E. Bauch, S. Singh, J. Lee, C.A. Hart, J.M. Schloss, M.J. Turner, J.F. Barry, L.M. Pham, N. Bar-Gill, S.F. Yelin, R.L. Walsworth, Decoherence of ensembles of nitrogen-vacancy centers in diamond, Phys. Rev. B. 102 (2020) 134210. https://doi.org/10.1103/PhysRevB.102.134210.

[30] C. Osterkamp, P. Balasubramanian, G. Wolff, T. Teraji, M. Nesladek, F. Jelezko, Benchmark for Synthesized Diamond Sensors Based on Isotopically Engineered Nitrogen-Vacancy Spin Ensembles for Magnetometry Applications, Advanced Quantum Technologies. n/a (2020) 2000074. https://doi.org/10.1002/qute.202000074.

[31] S. Kollarics, F. Simon, A. Bojtor, K. Koltai, G. Klujber, M. Szieberth, B.G. Márkus, D. Beke, K. Kamarás, A. Gali, D. Amirari, R. Berry, S. Boucher, D. Gavryushkin, G. Jeschke, J.P. Cleveland, S. Takahashi, P. Szirmai, L. Forró, E. Emmanouilidou, R. Singh, K. Holczer, Ultrahigh nitrogen-vacancy center concentration in diamond, Carbon. 188 (2022) 393–400. https://doi.org/10.1016/j.carbon.2021.12.032.

[32] P. Balasubramanian, C. Osterkamp, Y. Chen, X. Chen, T. Teraji, E. Wu, B. Naydenov, F. Jelezko, dc Magnetometry with Engineered Nitrogen-Vacancy Spin Ensembles in Diamond, Nano Lett. 19 (2019) 6681–6686. https://doi.org/10.1021/acs.nanolett.9b02993.

[33] A. Tallaire, J. Achard, F. Silva, O. Brinza, A. Gicquel, Growth of large size diamond single crystals by plasma assisted chemical vapour deposition: Recent achievements and remaining challenges, Comptes Rendus Physique. 14 (2013) 169–184.

[34] G. de Lange, T. van der Sar, M. Blok, Z.-H. Wang, V. Dobrovitski, R. Hanson, Controlling the quantum dynamics of a mesoscopic spin bath in diamond, Sci Rep. 2 (2012) 382. https://doi.org/10.1038/srep00382.

[35] T.R. Eichhorn, C.A. McLellan, A.C. Bleszynski Jayich, Optimizing the formation of depth-confined nitrogen vacancy center spin ensembles in diamond for quantum sensing, Physical Review Materials. 3 (2019) 113802. https://doi.org/10.1103/PhysRevMaterials.3.113802.

[36] A.M. Zaitsev, N.M. Kazuchits, V.N. Kazuchits, K.S. Moe, M.S. Rusetsky, O.V. Korolik, K. Kitajima, J.E. Butler, W. Wang, Nitrogen-doped CVD diamond: Nitrogen concentration, color and internal stress, Diamond and Related Materials. 105 (2020) 107794. https://doi.org/10.1016/j.diamond.2020.107794.

[37] K. Tahara, H. Ozawa, T. Iwasaki, N. Mizuochi, M. Hatano, Quantifying selective alignment of ensemble nitrogen-vacancy centers in (111) diamond, Appl. Phys. Lett. 107 (2015) 193110. https://doi.org/doi:http://dx.doi.org/10.1063/1.4935709.

[38] V. Stepanov, S. Takahashi, Determination of nitrogen spin concentration in diamond using double electron-electron resonance, Phys. Rev. B. 94 (2016) 024421. https://doi.org/10.1103/PhysRevB.94.024421.

SUPPLEMENTARY INFORMATION FILE FOR :

Enhancement of the creation yield of NV ensembles in a chemically vapour deposited diamond

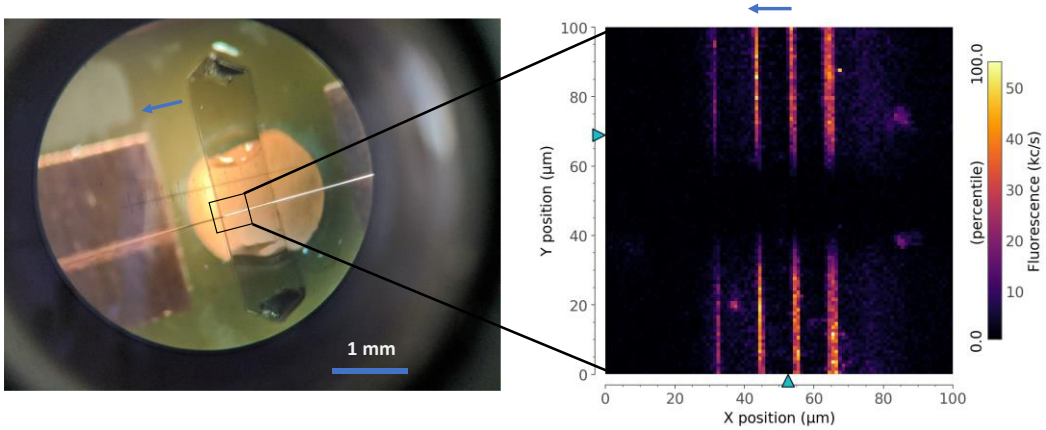

Fig. S1. (a) Image of the [113]-oriented diamond sample in cross-section under the confocal microscope. The wire used to bring microwave is visible across the sample. (b) Confocal microscopy photoluminescence map acquired in cross section showing the low-temperature layers as bright lines. The blue arrow indicates the growth direction. The inhomogeneous distribution of NV centres is evident with layers grown at lower temperature exhibiting higher luminescence. They are sandwiched between darker layers grown at higher temperature.

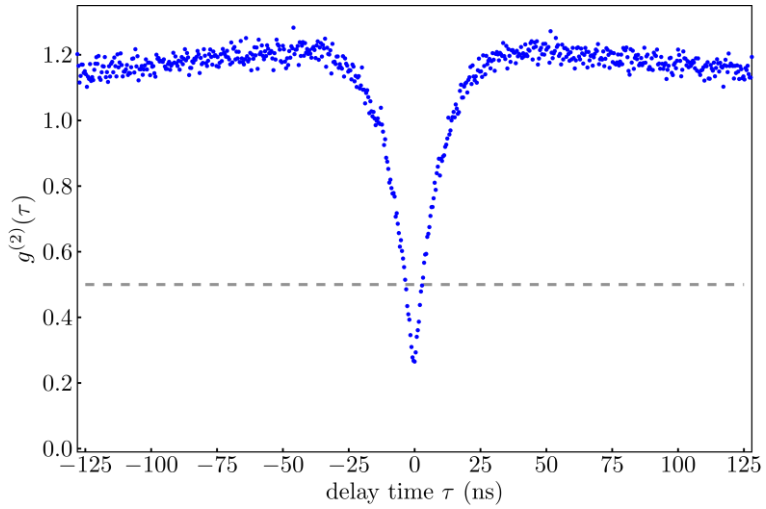

Fig. S2. Measured second order correlation function from a single NV centre. The intensity counts measured for such a single NV is used to assess NV density in the ensembles.

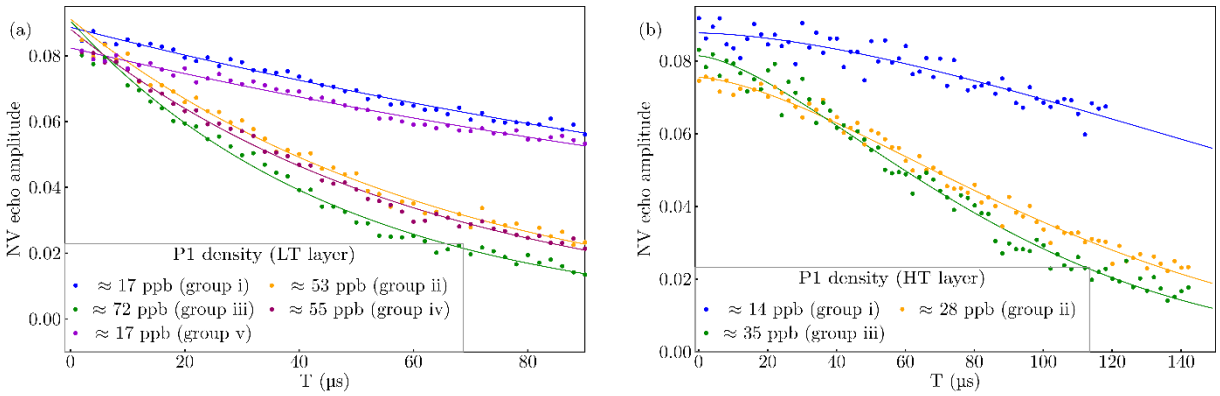

Fig S3 (a) Measurement of P1 bath density for the LT layer. The bath π-pulse is applied at all the transition frequencies (marked (i) – (v) in Figure 1c) of the P1 spectrum and the corresponding decay is recorded. The inter pulse spacing (τ_{fixed}) is kept as 100 μs. The measured data is fitted with the function of the form $\exp[-A\,\gamma_{NV}\gamma_{P1}n_{P1}T]$*, where* n_{P1} *gives the density of the measured P1 group. The total P1 density is calculated as* $n_{P1} = \sum_{\text{group=i}}^{\text{v}} n_{\text{group}}$*. (b) Measurement of P1 bath density for HT layer. The inter pulse spacing (τ_{fixed}) is kept as 150 μs and the decay is recorded for P1 group (i, ii and iii).* The total P1 density is calculated as $n_{P1} = n_{\text{iii}} + 2\,n_{\text{ii}} + +2\,n_i$.

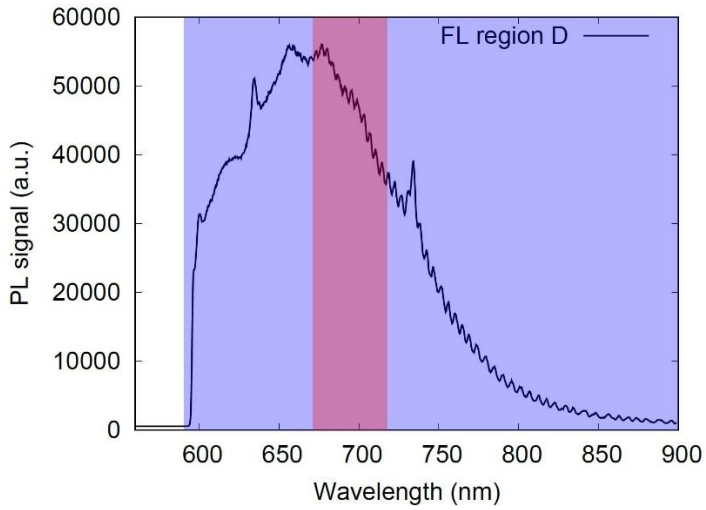

Fig. S4. Fluorescence spectrum of an ensemble of NV centres in the region D o the multi-layer sample. Blue and red areas correspond to the different filtering systems, and in particular to the detection band pass (580LP and 690/60BP) used to determine the NV centre density.

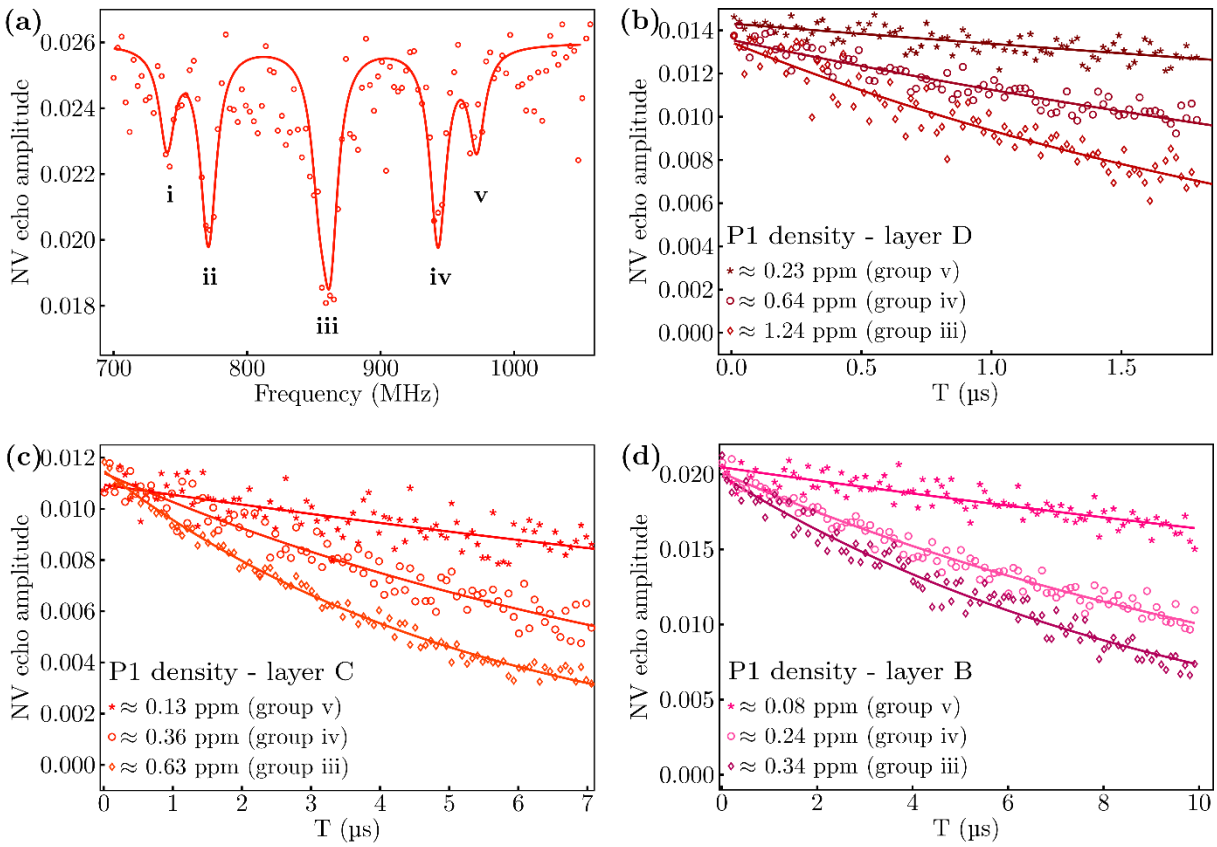

Fig. S5. (a) DEER spectrum obtained for layer C at an external magnetic field of 310 G aligned along the <111> crystal axis. The spectrum is obtained with NV echo inter-pulse spacing fixed at 3μs. (b) Measurement of P1 bath density for layer D. The echo inter-pulse spacing is fixed at 2.5μs. (c) Measurement of P1 bath density for layer C. The echo inter-pulse spacing is fixed at 7.5μs. (d) Measurement of P1 bath density for layer B. The echo inter-pulse spacing is fixed at 10.5μs.